

# Error Fields' Computation in the RFX-mod2 Reversed Field Pinch

Paolo Bettini<sup>1,2</sup>, Lionello Marrelli<sup>2</sup>, Dimitri Voltolina<sup>2</sup>, Roberto Cavazzana<sup>2</sup>, Giuseppe Marchiori<sup>2</sup>, Nicoló Marconato<sup>1,2</sup>, Ruben Specogna<sup>3</sup>, Gianluca Spizzo<sup>2</sup>, Riccardo Torchio<sup>1</sup>, and Paolo Zanca<sup>2</sup>

<sup>1</sup>Department of Industrial Engineering, University of Padova, 35131 Padua, Italy

<sup>2</sup>Consorzio RFX, 35127 Padua, Italy

<sup>3</sup>Polytechnic Department of Engineering and Architecture, Università di Udine, 33100 Udine, Italy

The aim of this article is to describe and model a sawtooth crash in RFX-mod2 and compute the eddy currents induced in the stabilizing shell surrounding the plasma for two alternative gap concepts and the subsequent error field. The sawtooth crash displacement of the plasma column is represented by a vacuum model coupled with a suitable magneto-quasi-static (MQS) volume integral (VI) formulation.

**Index Terms**—Eddy currents, error fields, integral formulations, magnetohydrodynamics (MHDs).

## I. INTRODUCTION

IN MAGNETIC confinement fusion, tokamaks are the most studied and have achieved the best overall performance. Nonetheless, other concepts have been developed: stellarator, reversed-field pinch (RFP), and compact torus concepts.

In this article, we deal with the error fields' computation in the RFX-mod, an RFP device ( $R = 2.0$  m and  $a = 0.459$  m), where a conducting structure (copper shell) close to the plasma is required to ensure the ideal stability of the RFP configuration [1]. Given the low value of the RFP safety factor ( $q \ll 1$ ) and the central peaking of current density, the RFP is characterized by the presence of several  $m = 1$  magnetohydrodynamics (MHDs) instabilities that, in RFX-mod, are controlled by a combination of passive structures and an active control system [2]–[4].

Nevertheless, the cuts in the shell (also named gaps), necessary for the penetration of electric and magnetic fields, locally distort the eddy current patterns generating error fields, i.e., deviations of the magnetic field from the axisymmetry, which may cause negative effects. In particular, when the component of an error field resonant with tearing modes (TMs)<sup>1</sup> is above a certain threshold, wall locking is forced, leading to localized plasma wall interaction.

In order to reduce MHD modes, a substantial enhancement of RFX-mod is in progress [5], consisting of the removal of the vacuum vessel (see Fig. 1) and in a major modification of the stainless steel toroidal support structure to make it vacuum-tight. In the new device (denoted as RFX-mod2), the shell-plasma distance will decrease by 10%, and the conducting surface closest to the plasma will become the copper shell.

Manuscript received November 30, 2020; revised February 3, 2021; accepted March 22, 2021. Date of publication March 30, 2021; date of current version May 17, 2021. Corresponding author: P. Bettini (e-mail: paolo.bettini@unipd.it).

Color versions of one or more figures in this article are available at <https://doi.org/10.1109/TMAG.2021.3069731>.

Digital Object Identifier 10.1109/TMAG.2021.3069731

<sup>1</sup>Tearing modes are perturbations of  $\vec{B}$  directed across the flux surfaces: the name itself comes from magnetic surfaces that are broken and reconnected in the form of magnetic islands.

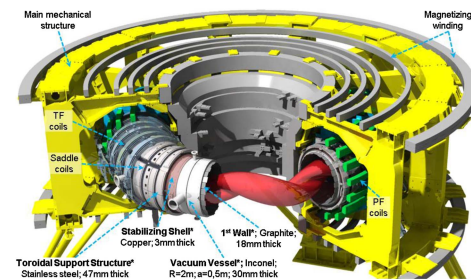


Fig. 1. Main conducting components surrounding the plasma in RFX-mod: stabilizing shell (copper, 3 mm), vacuum vessel (Inconel, 30 mm), and toroidal support structure (stainless steel, 47 mm). The main mechanical structure and coils (magnetizing winding, PF, TF, and saddle) are also shown.

As a result, MHD non-linear simulations predict a reduction of the amplitude of secondary TMs in RFX-mod2, and consequently, the edge bulging due to their phase locking is expected to decrease. Moreover, the plasma current threshold for TMs wall locking is expected to significantly increase [6].

On the other hand, due to the reduced shell-plasma distance, the RFX-mod2 plasma will be more sensitive to magnetic field errors at its boundary. The first study [7] confirmed that the overlapped poloidal gap concept [2], developed for RFX-mod, represents a significant improvement in terms of error field passive reduction compared to the original RFX butt-joint [8], and it has, therefore, been selected for RFX-mod2.

Moreover, RFX-mod2 might be prone to fast instabilities similar to those observed in the Madison symmetric torus (MST), an RFP device characterized by a highly conducting stabilizing shell located very near to the plasma. In MST, in fact, TMs are observed to rotate spontaneously in the kHz range, and regular sawtooth activity is observed: during a sawtooth cycle, the equilibrium current profiles slowly peak in the first phase and suddenly flatten at the crash phase [9].

The aim of this article is to compute the eddy current patterns and the subsequent error fields by simulating a sawtooth crash in RFX-mod2 considering either a butt-joint gap or an overlap gap and compare the relative error field spectra. The sawtooth crash displacement of the plasma column is

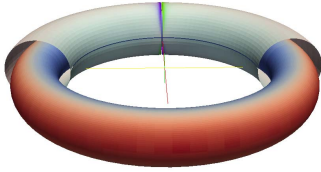


Fig. 2. Plasma is modeled by a thin sheet of current with periodicity  $m/n = 1/0$  spread on a toroidal surface with a minor radius of  $r = 35$  cm inside the vessel.

represented by a vacuum model introduced in Section II, coupled with a suitable magneto-quasi-static (MQS) volume integral (VI) formulation summarized in Section III.

## II. MODEL OF A RECONNECTION EVENT

The determination of sawtooth eddy currents adopts a simplified vacuum approach: the plasma is modeled with a thin sheet of current with periodicity  $m/n = 1/0$  flowing along a toroidal surface (minor radius  $r = 35$  cm) inside the vessel (see Fig. 2).

The current density on the surface is defined as

$$\mathbf{J}_p(\vartheta, \varphi) = \nabla\psi(\vartheta, \varphi) \times \hat{n} \quad (1)$$

where  $\hat{n}$  is the unit vector normal to the toroidal surface, and  $\vartheta$  and  $\varphi$  are the poloidal and toroidal coordinates, respectively.

The derivatives of the stream function  $\psi$  for an harmonic with periodicity  $m/n = 1/0$  are defined as

$$d\psi/d\theta = k, \quad d\psi/d\varphi = \cos(\vartheta + \omega t). \quad (2)$$

The constant  $k$  determines the amplitude of the current, and  $\omega$  is the angular frequency of rotation, used to solve the MQS problem in the frequency domain.

## III. MQS FORMULATION

As the time scale of sawtooth crashes is faster than the penetration of the equilibrium control field during the start-up phase, the diffusion of eddy currents through the thickness of the shell must be taken into account.

In this work, a suitable MQS VI formulation is adopted, which relies on the discrete geometric approach (DGA) and the use of the electric vector potential [10]; the electromagnetic fields are discretized on a pair of interlocked primal and dual grids of the conducting domain  $\Omega_c$  (copper shell).

The discrete Faraday's law is enforced on dual faces in  $\Omega_c$

$$\mathbf{C}^T \mathbf{U} + j\omega \mathbf{C}^T \mathbf{A} = 0 \quad (3)$$

where  $\mathbf{U}$  is the vector of the electro-motive forces (emf) on dual edges,  $\mathbf{A}$  stores the line integrals of the magnetic vector potential on dual edges, and  $\mathbf{C}$  is the standard incidence matrix between primal faces and edges. Then, the array of the currents across primal faces is defined as  $\mathbf{I} = \mathbf{C}\mathbf{T}$ , where the arrays  $\mathbf{T}$  store the unknown line integrals of the electric vector potential on primal edges.

Finally, the following discrete system is obtained:

$$\mathbf{K}\mathbf{T} = -i\omega \mathbf{C}^T \mathbf{A}_p \quad (4)$$

where  $\mathbf{A}_p$  is the term associated with  $\mathbf{J}_p$  defined in (1) and  $\mathbf{K} = \mathbf{C}^T (\mathbf{R} + j\omega \mathbf{M}) \mathbf{C}$ , with  $\mathbf{R}$  and  $\mathbf{M}$  being the resistance and magnetic matrices [10].

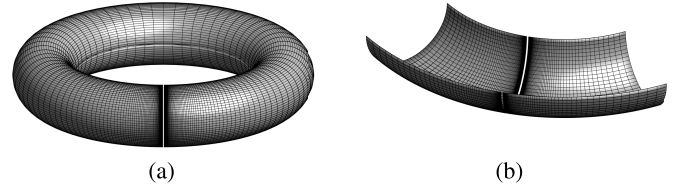


Fig. 3. *Butt-joint* gap concept: (a) Mesh of 76000 hexahedra. (b) Cut view of the gap region.

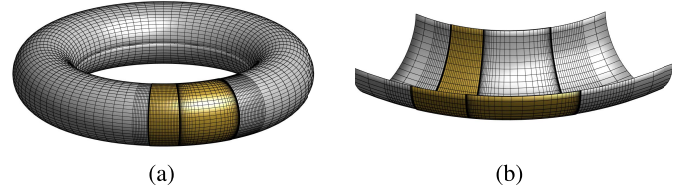


Fig. 4. *Overlapped* gap concept: (a) Mesh of 59280 hexahedra. (b) Cut view of the gap region.

TABLE I  
NUMBER OF ELEMENTS OF THE PRIMAL COMPLEX AND DOFS OF THE MODELS OF THE TWO ALTERNATIVE GAP CONCEPTS

		<i>butt-joint gap</i>	<i>overlap gap</i>
nodes	$N_n$	92826	72822
edges	$N_e$	261375	204637
faces	$N_f$	244550	191096
volumes	$N_v$	76000	59280
DoFs	$N$	135451	105305

## IV. NUMERICAL RESULTS

The numerical simulations are performed with the code CAFE-VI [10], which implements the formulation described in Section III, coupled with a low-rank approximation technique based on  $\mathcal{H}$ -matrix representation [11] used for assembling and solving the dense linear system (4). The results are also benchmarked in the lower frequency range to those obtained by the thin shell approximation implemented in the code CAFE-BEM [12].

### A. Alternative Gap Concepts

Two alternative gap concepts are considered: the butt-joint, which was proposed in RFX-mod2 preliminary design, being the easiest mechanical solution, and the overlapped, which has been selected as the final design, being the most effective in order to reduce error fields. The mesh in both cases is composed of hexahedra, with an appropriate mesh refinement in the gap region, as shown in Figs. 3 and 4; the number of elements of the primal complex (nodes, edges, faces, and volumes) and DoFs are shown in Table I.

Due to the low-rank approximation, the dense matrix  $\mathbf{K}$  in (4) is compressed from 280 to 10.5 GB for the butt-joint and from 169 to 9.7 GB for the overlapped, with a compression ratio of  $\rho_1 = 3.77\%$  and  $\rho_2 = 5.75\%$ , respectively.

### B. Eddy Current Patterns at High Frequency

The first numerical test consists of the characterization of eddy patterns at a given frequency to verify the sensitivity of the simulations to the mesh element size.

In toroidal regions far away from the gap, eddy currents are essentially toroidal, independently of the shell gap design.

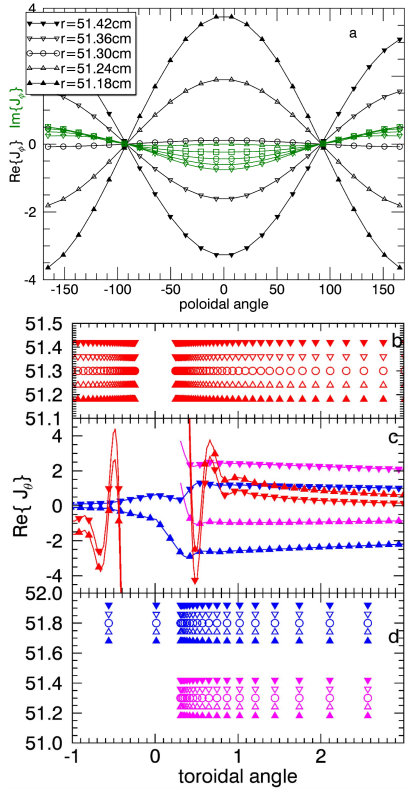


Fig. 5. (a) Poloidal dependence of the real (black) and imaginary (green) part of the toroidal current for the five layers composing the conducting shell. (b), (d) Radial position of barycenters of hexahedra in a toroidal region around the shell poloidal edges for butt joint (red) and overlapped shell (blue upper sheet and magenta lower sheet). (c) Toroidal dependence of the poloidal current: upper and lower triangles correspond to the inner layer and the outer layer, respectively.

Fig. 5 shows the poloidal dependence of the toroidal component for each layer of the mesh. The highest current occurs at the inner layer, which is nearer to the  $m/n = 1/0$  source (oscillating at 10 kHz in this case): the direction at  $\vartheta = 0$  (*low field side*) is opposite compared to that at  $\vartheta = 180$  (*high field side*) so that currents form a dipolar pattern. The toroidal current amplitude decreases in the middle layers, and it changes direction in the outer layers. In lower frequencies regimes ( $f < 1$  kHz), eddy currents in the layers are more uniform, and patterns are almost identical to the ones obtained by the thin shell approach [12].

Near the poloidal edges of the shell, the dominant eddy current component is the poloidal one for both gap concepts.

Fig. 5(c) shows the toroidal dependence of the poloidal current, which appears concentrated on two facing and anti-symmetric narrow layers and reaches very high values (40 in y-axis units) for the butt-joint (red triangles). The change of sign that takes place within half a degree from the gap edges does not appear to be an artifact of the discretization process, as the toroidal size of hexahedra is much smaller than this feature. Moreover, the poloidal current profile does not change by further reducing the toroidal size of hexahedra. As for the overlapped, the maximum value of poloidal current is located at the inner edge (magenta curves represent the inner sheet, blue curves represent the outer sheet, and upper and

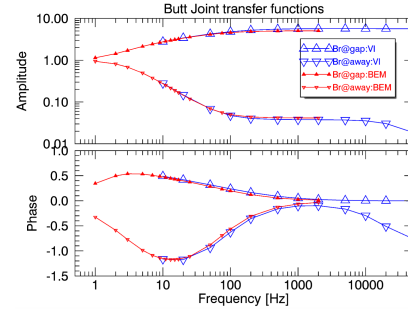


Fig. 6. *Butt-joint* gap: amplitude (top) and phase (bottom) of the radial field at plasma radius,  $\vartheta = 90^\circ$ .

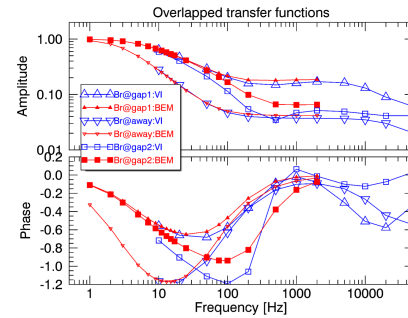


Fig. 7. *Overlapped* gap: amplitude (top) and phase (bottom) of the radial field at plasma radius,  $\vartheta = 90^\circ$ .

lower triangles indicate inner and outer layers, respectively), but it is ten times lower than in the butt-joint case. On the other hand, the poloidal current is distributed all along the overlapped region, and directions in the inner and outer layers are opposite for each sheet. This striking difference of current patterns has profound consequences on the radial magnetic field at the plasma surface of RFX-mod ( $r = 0.495$  m) and, consequently, the amplitude and (Fourier) spectrum of error fields.

The same problem is solved in a wide range of frequency; Figs. 6 and 7 show the transfer functions for the radial magnetic field in the butt-joint and overlapped configurations, in regions near the gap (upper triangles and squares) and far away (lower triangles) when the source is a toroidal surface with  $m/n = 1/0$  symmetry, as above.

Red traces represent the radial field computed by means of the thin shell approach [12], while the blue ones are obtained through the VI formulation presented in Section III. The two approaches yield similar results (at similar frequencies) for the butt joint case, while a greater attenuation and phase delay occurs for the radial field below the upper shell edge for the overlapped shell case.

### C. Error Fields Due to a Reconnection Event

The generic time evolution of the radial field at a given location is determined by Fourier decomposing the current-source time signal, multiplying by the transfer functions, and, finally, performing an inverse Fourier transform. As the first rough estimate, we consider an inward displacement of 0.5 cm: the Shafranov formula [7] gives an additional vertical field of 1 mT. In practice, we determine the current source time

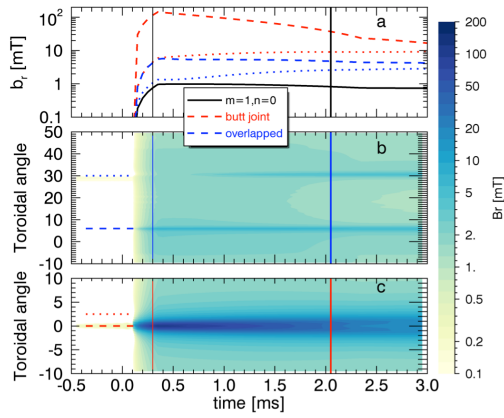


Fig. 8. Time evolution of radial error field during a reconnection event for overlapped (b) and butt joint (c) design. (a) Time traces in selected locations and the  $m = 1$ ,  $n = 0$  harmonic.

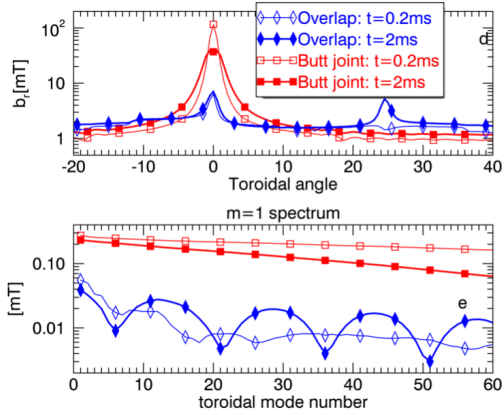


Fig. 9. Radial error field during a reconnection event. Top: error field profiles at  $t = 0.2$  ms and at 2 ms. Bottom: corresponding  $m = 1$  spectra.

behavior so that the  $m/n = 1/0$  harmonic of the radial field at plasma radius increases in  $250 \mu\text{s}$  and then remains constant [thick black trace in Fig. 8(a)].

Fig. 8(b) and (c) displays the time evolution of the radial field at the plasma surface of RFX-mod ( $r = 0.495$  m) and  $\vartheta = 90^\circ$  in a toroidal region around the shell edges (at  $\varphi = 0^\circ$  for the butt-joint and  $5^\circ$  and  $24^\circ$  in the overlapped shell). For the butt-joint, a very high radial field (up to 150 mT) is concentrated in a toroidal region extending few degrees. Though qualitatively similar to the error field shape during the start-up phase [6], it affects a narrower toroidal region. Red dashed and dotted time traces in panel a represent the time behavior of the field for two toroidal angles, as depicted in panel c. A significant reduction (by a factor 10–20) of the error field occurs in the *overlapped* concept (panel b). Interestingly, in the latter case, the error field evolves in two phases: initially (between 0.1 and 0.75 ms), only one peak occurs, located at the inner edge of the copper shell; later on, a second lower peak (outer edge of the overlapped shell) appears. The error field pattern of this later phase is also qualitatively similar to the start-up error described in [6].

The shape of the error field has important consequences on the  $m = 1$  harmonic spectrum (see Fig. 9), which influences

the dynamics of resonant MHD modes: for the butt-joint, it is almost flat, having a significant amplitude in the resonant interval  $n > 6$ . As time proceeds, the radial field peak broadens, and therefore, the higher  $n$  harmonics in the Fourier spectrum decrease. As far as the overlapped geometry is concerned, the Fourier spectrum in the first 0.5 ms is similar to the butt-joint case (i.e., monotonically decreasing) but significantly attenuated. Later on, 1 ms after the crash, it displays the characteristic interference pattern shown in Ref. [6] for a simulation of the RFX-mod2 start-up phase.

## V. CONCLUSION

In this work, a simulation of fast MHD phenomena for RFX-mod2 devices has been presented. The advanced numerical tools adopted here, i.e., an MQS VI formulation coupled with a vacuum model of a reconnection event, allowed demonstrating the dramatic difference between the overlapped and the butt-joint schemes on the fastest time scales. Even though the error field is highly localized in the first phase, its amplitude is significantly reduced in the overlapped scheme: this confirms that such a gap design, which is under implementation in RFX-mod2, is considerably better for an RFP boundary.

## ACKNOWLEDGMENT

This work has been carried out within the framework of the EUROfusion Consortium. This work was supported by the Euratom Research and Training Programme 2014–2018 and 2019–2020 under Agreement 633053. The views and opinions expressed herein do not necessarily reflect those of the European Commission.

## REFERENCES

- [1] L. Marrelli *et al.*, “The reversed field pinch,” *Nucl. Fusion*, vol. 61, no. 2, Jan. 2021, Art. no. 023001.
- [2] P. Sonato *et al.*, “Machine modification for active MHD control in RFX,” *Fusion Eng. Des.*, vols. 66–68, pp. 161–168, Sep. 2003.
- [3] R. Piovan *et al.*, “RFX machine and power supply improvements for RFP advanced studies,” *Fusion Eng. Des.*, vols. 56–57, pp. 819–824, Oct. 2001.
- [4] M. Zuin *et al.*, “Overview of the RFX-mod fusion science activity,” *Nucl. Fusion*, vol. 57, no. 10, Jun. 2017, Art. no. 102012.
- [5] S. Peruzzo *et al.*, “Technological challenges for the design of the RFX-mod2 experiment,” *Fusion Eng. Des.*, vol. 146, pp. 692–696, Sep. 2019.
- [6] L. Marrelli *et al.*, “Upgrades of the RFX-mod reversed field pinch and expected scenario improvements,” *Nucl. Fusion*, vol. 59, no. 7, Jul. 2019, Art. no. 076027.
- [7] L. Marrelli *et al.*, “Optimization of RFX-mod2 gap configuration by estimating the magnetic error fields due to the passive structure currents,” *Fusion Eng. Des.*, vol. 146, pp. 680–683, Sep. 2019.
- [8] G. Rostagni, “RFX: An expected step in RFP research,” *Fusion Eng. Des.*, vol. 25, no. 4, pp. 301–313, Jan. 1995.
- [9] A. F. Almagri, S. Assadi, S. C. Prager, J. S. Sarff, and D. W. Kerst, “Locked modes and magnetic field errors in the Madison symmetric torus,” *Phys. Fluids B, Plasma Phys.*, vol. 4, no. 12, pp. 4080–4085, Dec. 1992.
- [10] P. Bettini, M. Passarotto, and R. Specogna, “A volume integral formulation for solving eddy current problems on polyhedral meshes,” *IEEE Trans. Mag.*, vol. 53, no. 6, pp. 1–4, Feb. 2017.
- [11] R. Kriemann. *HLLIBpro* (v2.6). Accessed: Aug. 1, 2017. [Online]. Available: <https://hllibpro.com>
- [12] P. Bettini and R. Specogna, “A boundary integral method for computing eddy currents in thin conductors of arbitrary topology,” *IEEE Trans. Magn.*, vol. 51, no. 3, pp. 1–4, Mar. 2015.